



Clinical feasibility and impact of fully automated multiparametric PET imaging using direct Patlak reconstruction: evaluation of 103 dynamic whole-body ^{18}F -FDG PET/CT scans

André H. Dias¹ · Mette F. Pedersen¹ · Helle Danielsen¹ · Ole L. Munk^{1,2} · Lars C. Gormsen^{1,2}

Received: 22 May 2020 / Accepted: 18 August 2020 / Published online: 7 September 2020
© Springer-Verlag GmbH Germany, part of Springer Nature 2020, corrected publication 2021

Abstract

Purpose Functional imaging by standard whole-body (WB) ^{18}F -fluorodeoxyglucose (FDG) positron emission tomography (PET) is an integrated part of disease diagnostics. Recently, a clinical dynamic whole-body (D-WB) FDG PET/CT scanning protocols has been developed allowing for quantitative imaging of tissue metabolic rate of FDG (MR_{FDG}). It was the purpose of this retrospective study to evaluate whether MR_{FDG} imaging is feasible in a clinical setting and whether it improves lesion detectability.

Methods One hundred nine patients representing a broad range of referral indications for FDG PET/CT were invited to undergo a D-WB FDG PET/CT scan. Two sets of images were produced: parametric images and standard static SUV images. Both sets of images were reviewed visually, and 310 individual lesions were quantitatively analysed using the target-to-background (TBR) and contrast-to-noise (CNR) metrics.

Results One hundred three out of 109 patients completed the D-WB FDG PET/CT scan. There was no difference in the number of pathological lesions identified visually on the MR_{FDG} and the SUV images, whereas MR_{FDG} images yielded 4 fewer false positives than the SUV images. Quantitatively, MR_{FDG} TBR was significantly higher than SUV TBR in 299/310 lesions, and better MR_{FDG} CNR was found to facilitate the challenging reading of lesions with low SUV TBR.

Conclusion D-WB FDG PET/CT is feasible in a clinical setting and produces MR_{FDG} images of good visual quality and superior lesion contrast. In addition, MR_{FDG} images complement the standard SUV images providing better quantification and enhanced image reading. However, although MR_{FDG} also reduced the number of false-positive findings, no additional malignant lesions were identified. The technique therefore appears to be best suited for select patient groups or possibly treatment response evaluation.

Keywords Dynamic whole-body PET · FDG · Parametric imaging · Patlak · Oncology · Clinical

Ole L. Munk and Lars C. Gormsen contributed equally to this work.

This article is part of the Topical Collection on Oncology - General

Electronic supplementary material The online version of this article (<https://doi.org/10.1007/s00259-020-05007-2>) contains supplementary material, which is available to authorized users.

✉ Lars C. Gormsen
lars.christian.gormsen@clin.au.dk

¹ Department of Nuclear Medicine & PET Centre, Aarhus University Hospital, Palle Juul-Jensens Boulevard 165, DK-8200 Aarhus N, Denmark

² Department of Clinical Medicine, Aarhus University, Aarhus, Denmark

Introduction

Functional imaging by ^{18}F -fluorodeoxyglucose (FDG) positron emission tomography (PET) is an integrated part of diagnostics and follow-up of several malignant and non-malignant diseases [1–3]. FDG is a glucose analogue and therefore well suited to image glucose- and thus energy-consuming processes such as malignancy or activated inflammatory cells. Current FDG PET/CT imaging guidelines [4] advocate acquisition of static whole-body (WB) FDG PET/CT scan at a predefined time point, usually 60 min after tracer administration. PET/CT images are reviewed qualitatively for FDG uptake deemed pathological by thresholds set out in disease-specific guidelines or by local nuclear medicine physician experience. At times, a purely visual evaluation of FDG avidity may be supplemented by the standardized uptake value

(SUV), a semi-quantitative measure of glucose uptake [5]. This practice is logistically simple and has ensured a certain inter-observer and inter-institution reproducibility in producing and reading FDG PET/CT scans. However, although steadily increasing the use of static FDG PET/CT in diagnostic workups attests to the general usefulness of this approach, several methodological issues still inhibit the correct interpretation of the FDG PET/CT scans.

First, static FDG PET/CT represents a snapshot of accumulated tracer 60 min post-injection. Any information contained within the blood clearance of tracer or tissue tracer buildup is therefore by design lost and a lesion may appear more FDG avid solely due to delayed timing of the scan. Similarly, SUV images are dependent on many factors such as scanner calibration, non-perfect injections and the subject's body composition. From a clinical perspective, this is particularly problematic when FDG PET/CT is performed as part of treatment response evaluation [6, 7]. Second, static FDG PET imaging captures not only FDG-6-P retained in glucose consuming tissue but also a substantial background of unbound FDG in tissue and circulation. This may complicate the PET/CT evaluation of vascularized organs such as the liver, where lesions may not be visible above the background activity [8]. Third, although blood glucose levels should ideally be kept below 11 mmol/l at the timing of the FDG PET/CT injection [4], blood glucose excursions between 5 and 11 mmol/l may still impact on tissue radioactivity due to competitive uptake of endogenous glucose and FDG. This is most evident in the brain [9, 10] but may also affect FDG uptake by, e.g. tumours [11]. Collectively, these pressing issues concerning static FDG PET/CT warrant studies of how to optimize the imaging modality for clinical purposes. In this context, dynamic whole-body FDG PET/CT imaging of patients referred to PET/CT as part of diagnostic workup or treatment response evaluation is particularly appealing.

The use of dynamic imaging in PET is obviously not a novel concept [12] with literally thousands of published studies involving a wide range of tracers and analytical approaches. Traditionally, dynamic PET examinations were confined to a single-bed position with limited axial field-of-view and concurrent labour-intensive invasive blood sampling. Thus, despite the massive use in research settings, dynamic PET protocols have not translated into clinical oncology, where high-throughput WB PET/CT examinations are required for the assessment of disseminated disease. However, recent advances in PET scanner technology and software packages are about to change that [13]. The use of multi-pass, multi-bed PET acquisition has been used to perform dynamic WB (D-WB) imaging [14, 15] covering the entire body. The method acquires data non-continuously with time gaps between passes that is suitable for kinetic modelling using the linear Patlak analysis [16, 17] for estimation of the net irreversible uptake rate. It has been shown that invasive arterial

input blood sampling can be image-derived from voxels within the aorta or left ventricle [18]. Furthermore, new reconstruction algorithms [19] allow the creation of parametric images directly from PET sinogram data faster and with lower noise than traditional image-based methods.

While standard static FDG PET/CT produces a single SUV image, D-WB FDG PET/CT produces an *additional* output of two parametric images: the MR_{FDG} images, representing the metabolic rate of FDG into the tissue, and the DV_{FDG} images, representing the distribution volume of free FDG in the reversible compartments and the fractional blood volume. Whereas SUV images sum the entire FDG signal, the parametric images essentially allow for differentiation between free FDG and bound FDG-6-P.

So far, however, the clinical impact of D-WB PET scans has only been the subject of few studies, of which the largest included 118 lesions in 18 patients [20]. It is therefore still largely unexplored whether the introduction of D-WB with associated parametric images adds clinical information above and beyond what can be obtained by standard static FDG PET/CT. This information is of paramount importance since the replacement of a simple clinical method with a more laborious procedure should carry significant benefits to patients.

We performed both D-WB and static PET/CT's in a range of patients referred to FDG PET/CT on various indications. It was our goal with this review of 101 patients referred for a broad range of indications to evaluate (1) whether the acquisition of D-WB FDG PET is feasible in a clinical setting, (2) whether MR_{FDG} images are quantitatively superior to SUV images assessed by lesion target-to-background and contrast-to-noise measurements and (3) to determine if the acquisition of D-WB FDG PET/CT translates into clinical value in terms of improved lesion detection.

Materials and methods

Patient population

This was a retrospective study designed to evaluate D-WB FDG PET/CT and static FDG PET/CT lesion detection capability in patients referred to FDG PET/CT. Due to the retrospective nature of the study, individual patient consent was waived by the local ethics committee (Region Midtjylland). Access to patient files was granted by the Danish Patient Safety Authority (31-1521-59).

Patients were scheduled for the D-WB protocol if they were deemed fit to lie still for 70 min while in the PET/CT scanner. We attempted to scan a wide variety of patients and pathologies (see Table 1).

In total, we performed 103 complete D-WB PET/CT scans in 101 patients, and 310 lesions were evaluated. Two patients were scanned twice, at two different dates, when referred for

Table 1 Scan indications and demographic distribution of patient population

Scan indication	Number of patients			Age distribution*		
	Total	Male	Female	Total	Male	Female
Breast cancer	1	0	1	61	-	61
Cancer of unknown primary origin	6	3	3	62 [31–77]	56 [51–77]	68 [31–73]
Gynaecologic cancer	1	0	1	16	-	16
Head and neck cancer	3	2	1	55 [48–58]	51.5 [48–55]	58
Infection and inflammation	22	11	11	65 [18–91]	65 [47–91]	65 [18–72]
Lower digestive cancer	8	4	4	59 [55–78]	64 [55–78]	59 [56–71]
Lung cancer	36	18	18	67.5 [46–77]	67.5 [54–77]	67.5 [46–77]
Lymphoma	18	13	5	56.5 [22–77]	56 [22–77]	57 [41–73]
Testicular cancer	1	1	0	29	29	-
Upper digestive cancer	3	2	1	54 [53–55]	53.5 [53–54]	55
Urologic cancer	2	2	0	70.5 [70–71]	70.5 [70–71]	-
Total	101	56	45	65 [16–91]	65 [22–91]	65 [16–77]

*Values presented as median [range]

follow-up scanning according to standard PET clinical indication protocols in use at the hospital. Lesion pathology was verified by biopsy, other imaging modalities or clinical follow-up.

Data acquisition and image reconstruction

The patients were scanned using a fully automated multiparametric PET acquisition protocol (FlowMotion Multiparametric PET, Siemens Healthineers, Knoxville, USA) on a Siemens Biograph Vision 600 PET/CT scanner (Siemens Healthineers, Knoxville, USA) with 26.2-cm axial field-of-view.

Patients were informed about the prolonged examination procedure and comfortably placed in the scanner using positioning aid and supporting pillows [21]. Blood glucose level was measured, and an Intego PET Infusion System (MEDRAD, Inc., Warrendale, PA, USA) was connected to a peripheral venous catheter in the patient's arm. First, a low-dose WB CT (25 Ref mAs, 120 kV, CareDose4D, CareKV, Admire level 3) was performed. Then, the 70-min multiparametric PET acquisition protocol was started at the time of injection of FDG (4 MBq/kg). This protocol consisted of (1) a 6-min dynamic scan with the bed fixed at the chest region including organs as heart, liver and most importantly aorta and (2) a 64-min dynamic WB PET scan consisting of 16 continuous bed motion passes. For the first 60 patients, the bed speed of the WB passes was set to have 9×2 -min passes followed by 4×10 -min passes, and for the next 49 patients, the WB passes were set to have 7×2 -min WB passes followed by 9×5 -min WB passes. The total PET scan time including bed motion between the craniocaudal WB passes was 70 min. The process of data acquisition is shown in Fig. 1,

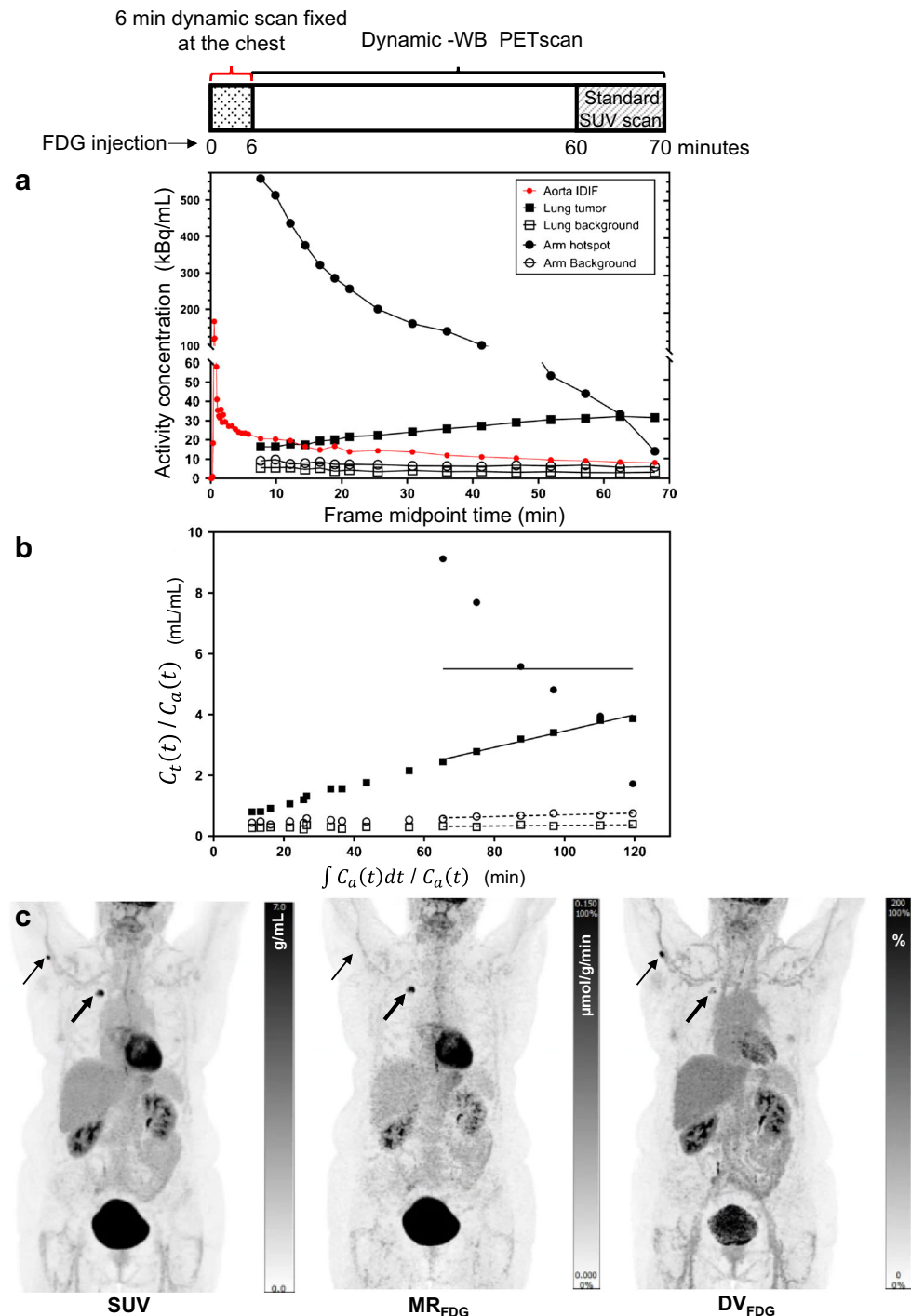
and the protocol generates both our standard-of-care static SUV image and additional parametric images.

Our standard-of-care static clinical PET images were reconstructed using PET software version VG76A and list-mode data from 60 to 70 min (reconstruction parameters: TrueX+TOF, 4 iterations, 5 subsets, 440 matrices, 2-mm Gaussian filter and relative scatter correction). The SUV images were normalized to body weight.

After PET data acquisition, the automated multiparametric scan protocol automatically identified aorta on the low-dose WB CT scan [22] and placed a VOI (1.6 mm³ cylinder) from which an arterial image-derived input function (IDIF) was extracted from the full dynamic PET series of the chest region, i.e. the first 6 min, combined with the chest region of the subsequent WB passes. The automated aorta landmarking failed in one patient, and we had to manually outline the aorta VOI.

The multiparametric scan protocol generates parametric images based on the Patlak model that assumes a single arterial input function, any number of reversible compartments and an irreversible compartment where tracer remains bound. The Patlak model is only valid after some time when the free tracer has reached a steady state between blood and tissue. The parameters are the Patlak slope (K_i), which is the rate of irreversible uptake, and the Patlak intercept (DV), which is the apparent distribution volume of non-metabolized tracer [16, 17]. In this study, we used the patient's measured blood glucose to obtain the metabolic rate of FDG, $MR_{FDG} = K_i \times \text{blood glucose}$. Parametric images of MR_{FDG} and DV_{FDG} were generated using the nested direct Patlak reconstruction method [23] using list-mode data from the 6 last passes, i.e. 40–70 min, and the automatically generated IDIF (reconstruction parameters: TrueX+TOF, 8 iterations, 5 subsets, 30 nested

Fig. 1 All patients were scanned using a 70-min D-WB PET/CT protocol consisting of 6-min dynamic PET scans of the chest region followed by a 64-min D-WB PET scan. Low-dose CT scans were acquired before and after the PET scans. The combination of the full aorta input curve, (red curve in graph **a**) with the late tissue activity curves (black curves in graph **a**), allows the use of the Patlak linearization (**b**) for multiparametric imaging (**c**). SUV images are reconstructed using D-WB data from 60 to 70 min, whereas the parametric images of MR_{FDG} and DV_{FDG} are reconstructed using D-WB data from 40 to 70 min. Note on graph **a** how SUV values at 60 min are similar for the lesions in the upper arm and lung, whereas the time-activity curves are markedly different, which is revealed in the multiparametric images. This results in a false-positive finding on SUV (thin arrows) in the right upper arm of a patient with lung cancer (thick arrows). Further investigation with ultrasound and biopsy did not identify any malignancy in the area, as was suggested by MR_{FDG} and DV_{FDG} images



loops, 440 matrices, 2-mm Gaussian filter and relative scatter correction).

Image analysis

Visual

Parametric Patlak images of MR_{FDG} and DV_{FDG} were visually compared with standard 60-min static SUV

images using Hermes® (V0413) (Hermes Medical Solutions AB, Stockholm, Sweden). Visual comparisons (sharpness of contours, noise and lesion detectability) were performed by two nuclear medicine physicians (AHD with 6 years of PET experience and LCG with 12 years of PET experience). The semi-quantitative analysis and analysis of dynamic images were performed by AHD using PMOD® 4.0 (PMOD Technologies Ltd., Zürich, Switzerland).

Quantitative

In all D-WB studies, representative target lesions were selected by AHD. A VOI was drawn around the respective regions and PMOD's isocontour tool was used (threshold set to 50% of max) to obtain the final target region. Background regions were manually drawn in adjoining tissue. Lesion detectability by a human observer is a complex task depending on signal, background, noise, shape, size, location and experience. We used target-to-background ratio (TBR) and contrast-to-noise ratio (CNR) as two objective metrics for quantitative assessment of image quality in terms of "lesion detectability". TBR for mean and max is given as:

$$TBR_{\text{MEAN}}(\text{signal}) = \frac{\text{MEAN}(\text{target signal})}{\text{MEAN}(\text{background signal})}$$

$$TBR_{\text{MAX}}(\text{signal}) = \frac{\text{MAX}(\text{target signal})}{\text{MEAN}(\text{background signal})}$$

which we measured on SUV images, $TBR_{\text{MEAN}}(\text{SUV})$ and $TBR_{\text{MAX}}(\text{SUV})$, and on parametric MR_{FDG} images, $TBR_{\text{MEAN}}(MR_{\text{FDG}})$ and $TBR_{\text{MAX}}(MR_{\text{FDG}})$. Detectable lesions must have a $TBR > 1$, and higher TBR indicates better lesion detectability except in special cases with low-target signal combined with extremely low background signal.

CNR is the lesion contrast (target signal – background signal) divided by noise (standard deviation in the background, $\sigma_{\text{background}}$). CNR for mean and max is given as:

$$\begin{aligned} CNR_{\text{MEAN}}(\text{signal}) \\ = \frac{\text{MEAN}(\text{target signal}) - \text{MEAN}(\text{background signal})}{\sigma_{\text{background}}} \end{aligned}$$

$$\begin{aligned} CNR_{\text{MAX}}(\text{signal}) \\ = \frac{\text{MAX}(\text{target signal}) - \text{MEAN}(\text{background signal})}{\sigma_{\text{background}}} \end{aligned}$$

which we measured on SUV images, $CNR_{\text{MEAN}}(\text{SUV})$ and $CNR_{\text{MAX}}(\text{SUV})$, and on parametric MR_{FDG} images, $CNR_{\text{MEAN}}(MR_{\text{FDG}})$ and $CNR_{\text{MAX}}(MR_{\text{FDG}})$. Higher CNR indicates better lesion detectability.

A total of 310 target regions (VOIs) were analysed. Target areas were visually assessed from PET images and classified into benign, equivocal benign/malign or malign. This visual evaluation was afterwards compared with reference standards, such as results from biopsy, evaluation and evolution of the lesions in complementary imaging techniques and with clinical information and follow-up.

Statistical analysis

The statistical and graphical analysis of the extracted data were performed using Stata 16 and Graphpad Prism 8.4.2. Comparison of $TBR_{\text{MEAN}}(MR_{\text{FDG}})/TBR_{\text{MEAN}}(\text{SUV})$ ratios between disease categories was done by Kruskal-Wallis (for group comparisons of more than two) or the Mann-Whitney test (for post hoc non-paired comparisons). $CNR_{\text{MEAN}}(MR_{\text{FDG}})/CNR_{\text{MEAN}}(\text{SUV})$ ratios were tested against a median of 1 using the Wilcoxon signed-rank test for each individual group. Spearman's rank correlation was used to assess the relationship between SUV and K_i . In all the tests, a p value < 0.05 was considered significant.

Results

Clinical feasibility of D-WB scanning

D-WB PET scans were scheduled for the first patient slot of the day. Thus, the long examination time did not delay the daily schedule as participating patients were simply injected while placed in the scanner instead of in a bed in the designated "uptake" room. Thorough scan procedure information and careful patient handling and positioning were crucial to make patients feel comfortable and enable the prolonged 70-min examination [21]. The first 30 patients were scanned with arms down, but subsequent patients were scanned with their arms above the head. Of the first 109 multiparametric scans, 103 were successful (and analysed in this paper), and 6 failed (2 patients became ill, 3 patients had to visit the restroom and the Intego injector failed once). In all 6 cases, where the multiparametric scan had to be interrupted, the patients were able to receive the standard-of-care 60–70 min static WB PET scan after a short break.

Biopsy results

Ninety-seven out of 103 PET scans had areas considered of interest by the study researcher, including both benign and malignant areas. Six scans were without areas of pathological FDG uptake on the SUV images or signal above background on the MR_{FDG} images and no VOIs were consequently drawn on these. A total of 310 VOIs (lesions) were analysed, of which 120 lesions were of benign appearance, 17 lesions of equivocal appearance (benign or malign) and 173 lesions suspect of malignancy. Verification (biopsy, imaging or clinical) of these 310 lesions is presented in Table 2.

Visual appearance of the scans

All D-WB PET images were rated of visual good quality (resolution, sharpness of contours, noise, presence of artefacts) by both reviewers and were comparable with standard

static SUV images as shown in the examples below (Fig. 2a–d). In general, MR_{FDG} images were by design characterized by absent or sharply reduced signal in vascularized tissues (liver, mediastinum, spleen, large vessels and renal pelvises) and with a tendency towards slightly increased signal intensity

Table 2 Distribution of VOIs by visual assessment of PET images and subsequent confirmation by reference standards

Scan indication	Total of patients	Visual PET assessment of VOIs	Biopsy	Imaging	Clinical	No follow-up	Total	VOI total
Breast cancer	1	Benign	-	-	-	-	-	4
		Benign/malign	-	-	-	-	-	-
		Malign	4	-	-	-	4	-
CUPO*	6	Benign	1	-	3	-	4	12
		Benign/malign	-	-	-	-	-	-
		Malign	7	-	-	1	8	-
Gynaecologic cancer	1	Benign	-	-	1	-	1	3
		Benign/malign	-	-	-	-	-	-
		Malign	2	-	-	-	2	-
Head and neck cancer	3	Benign	1	3	-	-	4	6
		Benign/malign	-	-	-	1	1	-
		Malign	1	-	-	-	1	-
Infection and inflammation	22	Benign	5	1	53	-	59	61
		Benign/malign	-	-	1	-	1	-
		Malign	-	-	1	-	1	-
Lower digestive cancer	8	Benign	-	3	5	-	8	29
		Benign/malign	-	1	-	-	1	-
		Malign	18	2	-	-	20	-
Lung cancer	36	Benign	1	6	15	-	22	127
		Benign/malign	4	4	2	2	12	-
		Malign	86	6	-	1	93	-
Lymphoma	18	Benign	4	2	14	-	20	56
		Benign/malign	1	1	-	-	2	-
		Malign	27	6	-	1	34	-
Testicular cancer	1	Benign	-	-	-	-	-	1
		Benign/malign	-	-	-	-	-	-
		Malign	1	-	-	-	1	-
Upper digestive cancer	3	Benign	-	-	1	-	1	7
		Benign/malign	-	-	-	-	-	-
		Malign	3	2	-	1	6	-
Urologic cancer	2	Benign	-	-	-	-	1	4
		Benign/malign	-	-	-	-	-	-
		malign	3	-	-	1	3	-
Total	101		170	37	96	8	310	

*CUPO, cancer of unknown primary origin

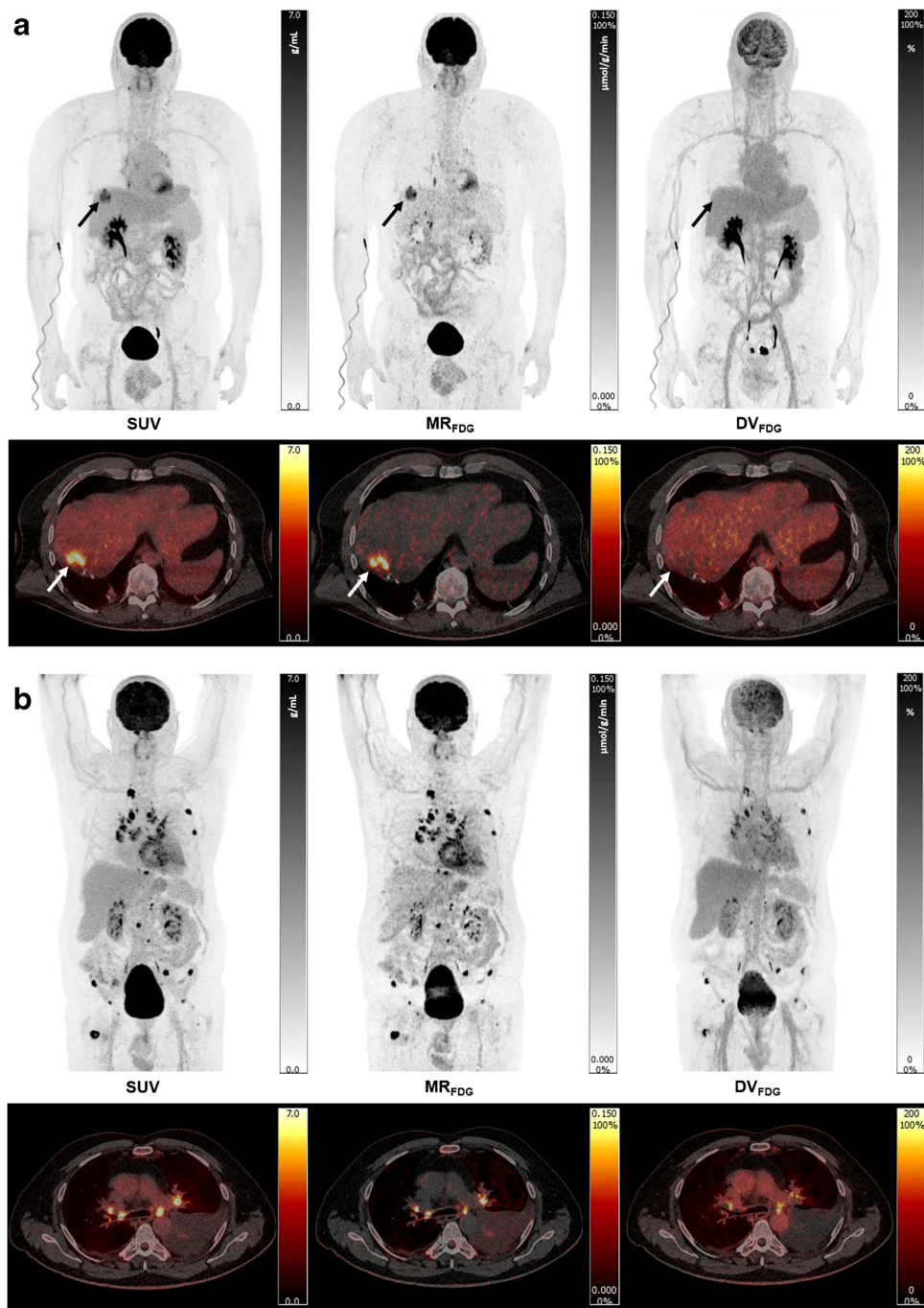


Fig. 2 **a** Example of enhanced detectability of hepatic lesions caused by reduced vascular background. The patient suffered from relapsing colon cancer with single liver metastasis (arrow). The MR_{FDG} image shows better TBR than the SUV image. **b** Example of significant free FDG in the malignant lesions clearly visible on the DV_{FDG} image. The patient was diagnosed with adenocarcinoma of the lung. PET showed disseminated disease with multiple pulmonary, lymph node and bone metastases. Note on MR_{FDG} images the improved mediastinal lymph nodes target-to-background when compared with the SUV image but also the marked signal in the bone metastases on the DV_{FDG} image. **c** Example of almost exclusively irreversible FDG uptake by malignant lesions.

Lesions are clearly visible on the MR_{FDG} image and to a large extent absent on the DV_{FDG} image. The patient suffered from an adenocarcinoma of the rectum with soft tissue metastases in the pelvis as well as dissemination to mediastinal lymph nodes, the lungs and the liver (arrow). **d** Example of a patient with non-malignant disease. The patient was referred to suspicion of malignant lymphoma and the PET scan revealed avid FDG uptake in multiple enlarged lymph nodes in the mediastinum and a conglomerate of lymph nodes on the right side of the abdomen. Biopsy from the abdominal conglomerate showed only granulomatous/inflammatory changes, and the patient is currently being treated for sarcoidosis with good clinical response

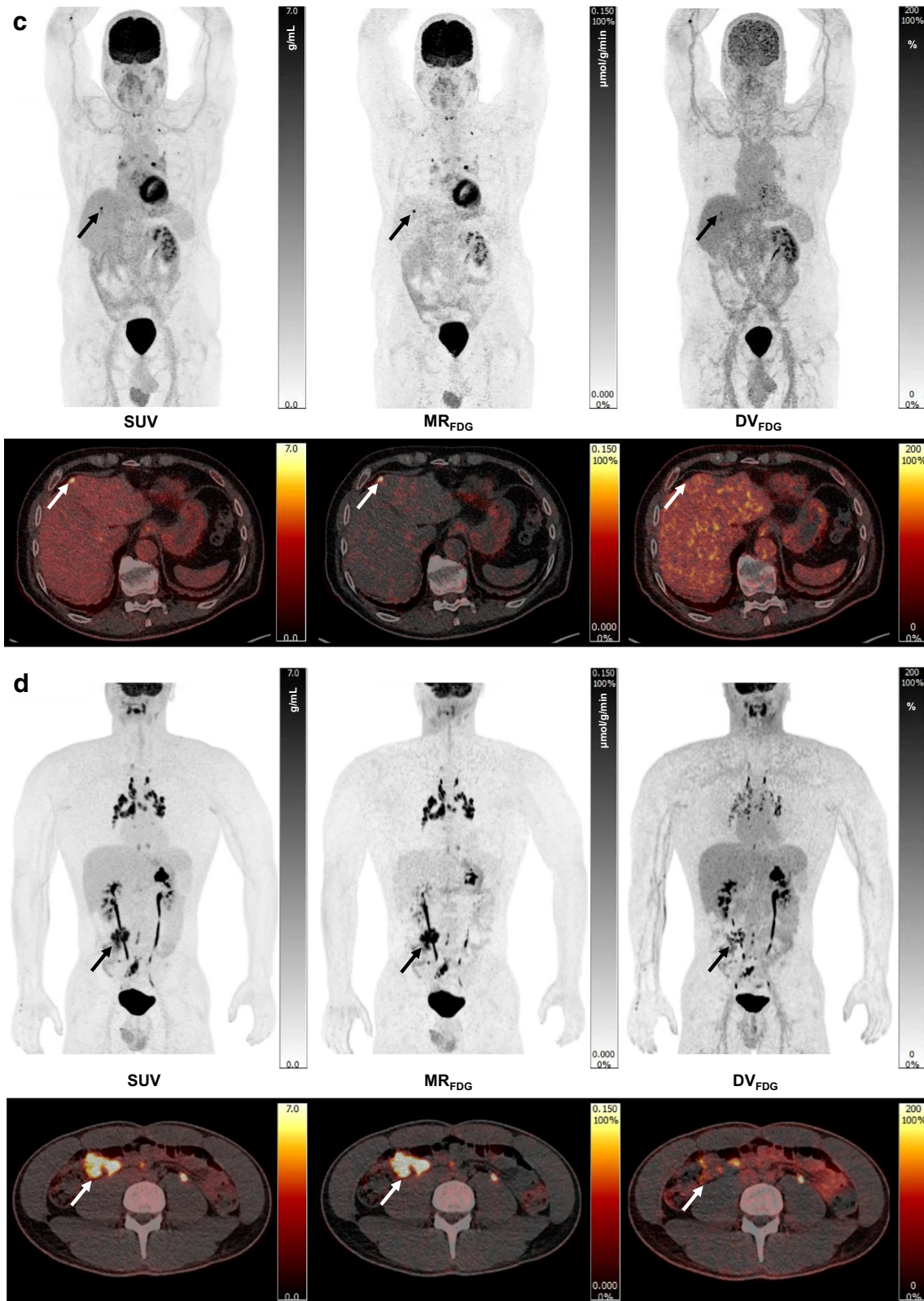


Fig. 2 (continued)

from the gastric ventricle and intestines. The DV_{FDG} images were characterized by high-signal intensity in the vascularized organs not visible on the MR_{FDG} images but also by some signal from both benign and malignant lesions.

Visual lesion detection

Overall, visual lesion detection in terms of the number of identified lesions was almost identical in MR_{FDG} images and SUV images, with a few notable exceptions. In four patients, SUV images revealed FDG avid foci in soft tissue or adjoining vessels, which could not confidently be written off as artefacts. In one patient with pulmonary cancer, shown in Fig. 1, several biopsies were made to ensure that a subcutaneous SUV image FDG avid focus was not a metastasis. These foci were completely absent from the MR_{FDG} images and visible on the DV_{FDG} images indicating (correctly) that the SUV image FDG avidity was due to free tracer. However, although the absence of background activity in, e.g. the liver and the mediastinum facilitated easier reading of the MR_{FDG} images, no *additional* pathological lesions were identified.

We next evaluated whether lesions deemed “benign” or “malignant” appeared qualitatively different on the MR_{FDG} images than on SUV images. This was not the case: as seen in Fig. 2b, malignant metastases from pulmonary cancer appeared with the same signal intensity on SUV and MR_{FDG} images and correspondingly, no visual difference was observed in the appearance of benign granulomatous lesions (Fig. 2d).

Figure 3 shows the relation between quantitative ($K_{i,mean}$) and semi-quantitative (SUV_{mean}) measurements of lesion metabolism. As seen, there was generally an excellent correlation between SUV and K_i (Spearman $r = 0.93$) with a few malignancies deviating from the line of identity. Of interest and as expected, fast-growing and cell-rich malignancies such as

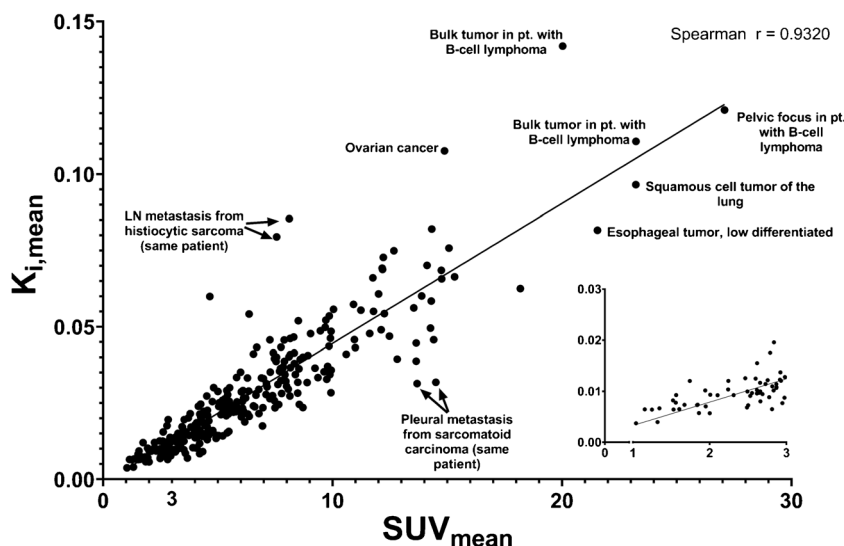
lymphomas and histiocytic sarcomas had K_i values above the line of identity, whereas vascularized malignancies such as sarcomatoid tumours had K_i values below the line of identity.

Quantitative lesion target-to-background analysis

As seen in Fig. 4, the observed lesion TBR was superior in the MR_{FDG} images as indicated by the location of 299/310 lesions above the line of identity. The most pronounced difference in lesion TBR between MR_{FDG} images and SUV images was observed in metastases from pulmonary cancer and lymphoma lesions where TBR for MR_{FDG} images were as high as 150. In the lower range of TBR, where lesions may be more difficult to discriminate from a background (Fig. 4c), there was no apparent pattern in the distribution of malignant and benign lesions. The 11 lesions with higher SUV TBR than MR_{FDG} TBR were predominantly benign lesions.

We next evaluated whether lesion TBR distribution was influenced by the histology of lesions. This was done by dividing $TBR_{MEAN}(MR_{FDG})$ with the $TBR_{MEAN}(SUV)$ and comparing this index between disease groups. Any value above 1 indicates more intense lesions in the MR_{FDG} images. As seen in Fig. 5, $TBR_{MEAN}(MR_{FDG})/TBR_{MEAN}(SUV)$ ratio was significantly higher in some malignant lesions (notably GI cancers and pulmonary cancers) than in the inflammatory and infectious (benign) lesions. Also, when comparing all malignant lesions with benign lesions, $TBR_{MEAN}(MR_{FDG})/TBR_{MEAN}(SUV)$ ratio was significantly higher (right panel). However, although $TBR_{MEAN}(MR_{FDG})$ thus appeared to be predominantly higher in the malignant lesions on a group level, there was a significant overlap on individual lesion level. In short, TBR levels cannot be used to distinguish between benign and malignant lesions.

Fig. 3 Correlation of SUV_{mean} and $K_{i,mean}$. Insert containing the lower range of SUV_{mean} . The 4 false-positive outliers were removed from this plot



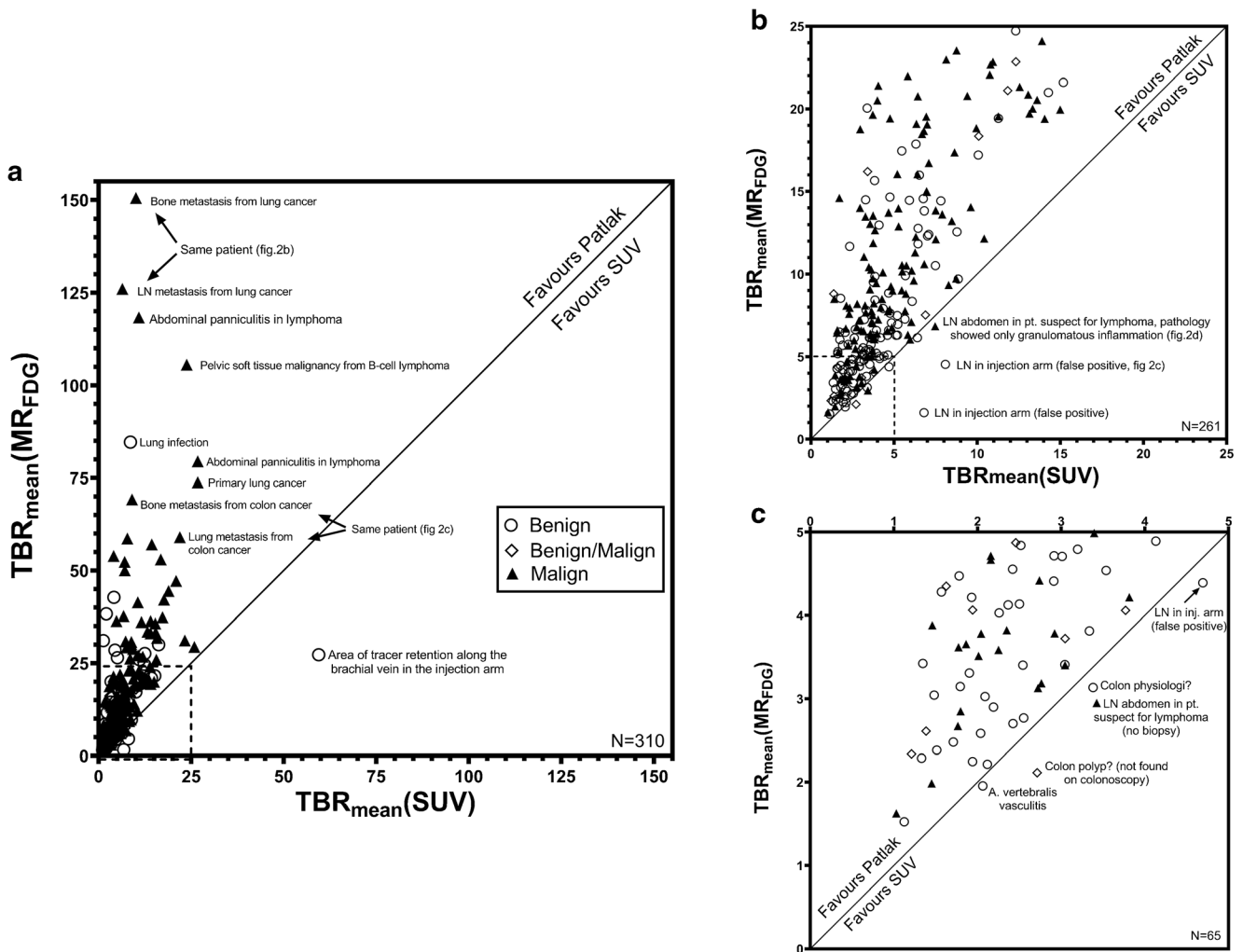


Fig. 4 Distribution of analysed volumes of interest by classification into “benign”, equivocal “benign/malign” and “malign” showing a clear predominance of lesions favouring MR_{FDG} imaging. Graph a with the

distribution of all VOIs ($N = 310$), **b** with zoom on area 25×25 TBR ($N = 262$), **c** with zoom on area 5×5 TBR ($N = 67$)

Finally, we explored whether quantitative image quality represented by CNR differed between D-WB and static PET (the ratio between $CNR_{MEAN}(MR_{FDG})$ and $CNR_{MEAN}(SUV)$). This can be considered a measure of the “image readability” and the value 1 represents equality between the two approaches. We did this under four different and challenging clinical circumstances: (1) low background/low TBR (representing, e.g. adenocarcinoma of the lungs), (2) low background/high TBR (representing, e.g. squamous cell carcinoma of the lungs), (3) high background/low TBR (e.g. splenic marginal zone lymphoma), (4) high background/high TBR (hepatic metastasis). We chose a mean $SUV = 2$ and $TBR_{MEAN}(SUV) = 2$ as the cutoff between high and low background and TBR. As seen in Fig. 6, groups 1 and 3 had $CNR_{MEAN}(MR_{FDG})/CNR_{MEAN}(SUV)$ significantly above 1, and group 3 had $CNR_{MAX}(MR_{FDG})/CNR_{MAX}(SUV)$ significantly above 1, indicating that lesions characterized by a low TBR are more easily detected on the MR_{FDG} images.

Representative examples of lesions in group 3 and plots of $CNR(MR_{FDG})$ vs $CNR(SUV)$ are shown in the [supplemental material](#).

Discussion

This retrospective study demonstrates that fully automated multiparametric WB FDG PET imaging is feasible in a clinical setting as demonstrated by our 103/109 successful scans. The resultant MR_{FDG} images are of visual good quality in terms of sharpness, background noise and resolution, and quantitative lesion TBR(MR_{FDG}) is superior to TBR(SUV). In addition, parametric imaging of “free” tracer by the DV_{FDG} images allows for correct identification of small SUV image foci as artefacts increasing the specificity of FDG PET/CT. However, the quantitative superiority in lesion detection by MR_{FDG} imaging does not translate into the

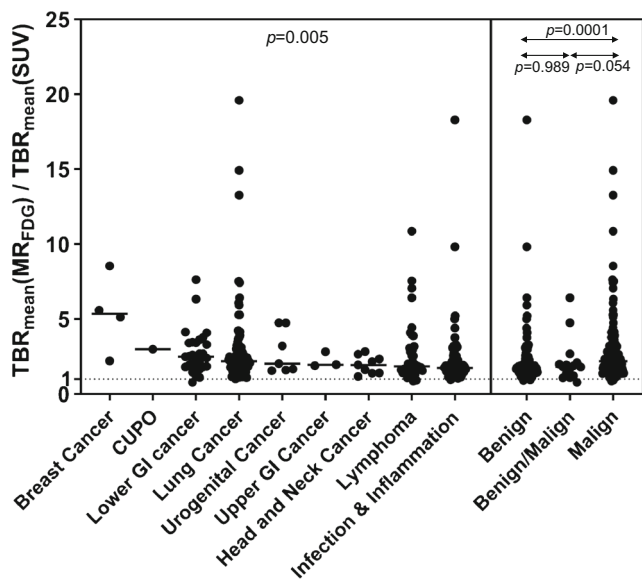


Fig. 5 $TBR_{MEAN}(MR_{FDG})/TBR_{MEAN}(SUV)$ comparison between individual disease subtypes as well as between the visual classification categories of “benign”, equivocal “benign/malign” and “malign” lesions. Comparison of $TBR_{MEAN}(MR_{FDG})/TBR_{MEAN}(SUV)$ ratios between disease categories was done by Kruskal-Wallis (for group comparisons of more than two) or the Mann-Whitney test (for post hoc non-paired comparisons). Comparison between visual classification categories was done by the Mann-Whitney test

detection of *more* lesions, i.e. the sensitivity of MR_{FDG} imaging is equal to SUV imaging, at least in a patient cohort containing a significant proportion of oncological staging scans. Also, although MR_{FDG} imaging generally produces greater lesion TBR in malignant than in benign lesions, lesion TBR alone cannot be used to distinguish between benign and malignant lesions. There may be several explanations for our observed comparable clinical performance of standard SUV and multiparametric FDG PET imaging. As shown in Fig. 3, we observed an excellent correlation between SUV and K_i . The benefit of parametric images is essential that they allow for differentiation between reversible free FDG in the blood (DV_{FDG}) and the irreversible uptake in the form of FDG-6-P (MR_{FDG}), whereas SUV represents the combined signal. Thus, a signal in the MR_{FDG} image is always associated with a SUV signal (and not the other way around). Whether the SUV value is recognized as a signal of pathology largely depends on the background activity, i.e. the free unbound FDG. In this regard, it is of interest that our patient cohort was characterized by a large fraction of patients suffering from pulmonary cancers and thoracic inflammatory diseases, where the pathological lesions were primarily located in tissue devoid of free background FDG activity. In these patients, the comparable lesion detectability was therefore foreseeable.

Similar deliberations have previously led others to suggest a more targeted approach to the use of parametric imaging. Karakatsanis et al. [14, 24] divided oncology FDG PET

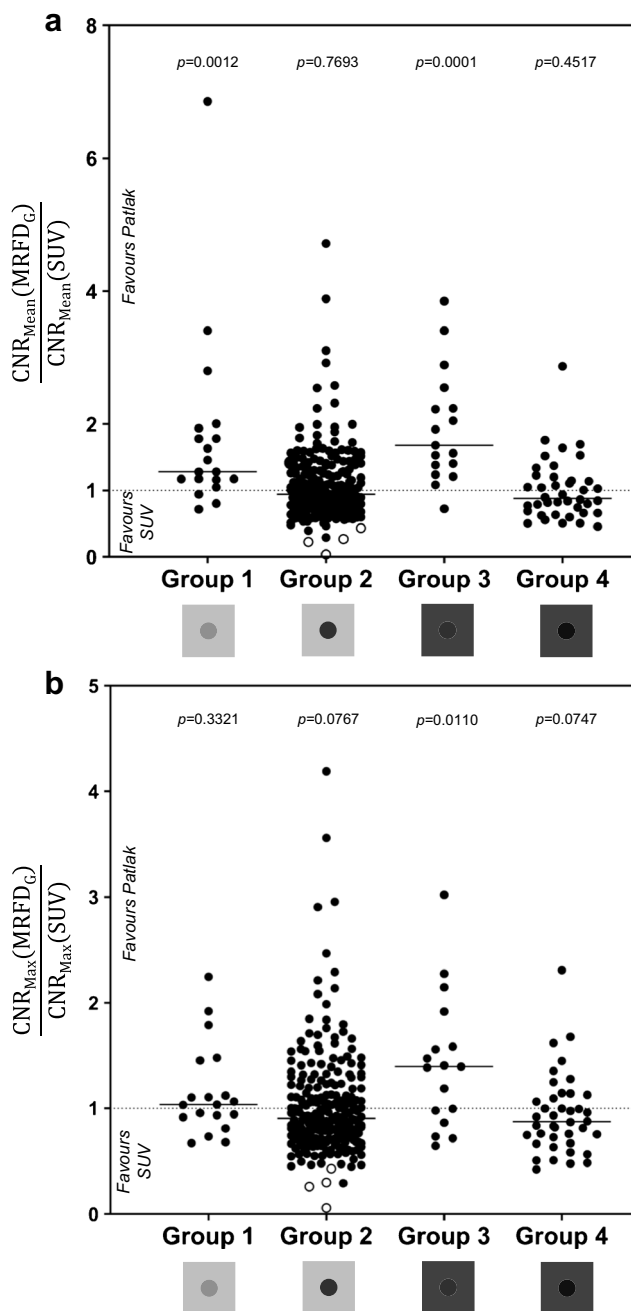


Fig. 6 $CNR_{MEAN}(MR_{FDG})/CNR_{MEAN}(SUV)$ ratios (a) and $CNR_{MAX}(MR_{FDG})/CNR_{MAX}(SUV)$ ratios (b) divided into groups under four different and challenging clinical circumstances based on SUV: (1) low background/low TBR, (2) low background/High TBR, (3) high background/low TBR, (4) high background/high TBR. We chose a mean $SUV = 2$ and also $TBR = 2$ as the cutoff between high and low background and TBR. Displayed p values represent the result of the Wilcoxon signed-rank test for each individual group against a median of 1. The four open circles are false positives. The CNR_{MEAN} plot (a) shows 151 points over 1 and 159 points under 1. The CNR_{MAX} plot (b) shows 182 points above 1 and 128 points below one. Thus, contrast-to-noise was better for MR_{FDG} than SUV in around half of the lesions, which indicate that the D-WB examination (with both SUV and MR_{FDG} images) leads to improved detection of these lesions

studies into three categories: (a) high-uptake tumours surrounded by high and constant background activity, (b) low-uptake tumours surrounded by low background activity and (c) high-uptake tumours surrounded by low background. According to Karakatsanis et al., MR_{FDG} is most likely of additional value in the case of high-uptake tumours surrounded by high background activity, whereas it is less likely that MR_{FDG} adds further useful clinical information in the case of low-uptake tumours—even when background activity is low. Of interest and in line with our findings, they also observed negligible value of MR_{FDG} in pulmonary cancers compared with standard SUV imaging.

However, even in patients with fast-growing malignancies characterized by metastases to the liver (corresponding to group a in the above), we observed no additional lesions on the MR_{FDG} images. As depicted in Fig. 2a and c, patients with hepatic metastases from colorectal cancers had lesions clearly visible on SUV images despite significantly poorer TBR than in the MR_{FDG} images. Colorectal malignancies are generally fast growing reflected by a high Ki-67 index [25] and consequently, glucose and FDG uptake by hepatic metastases is considerable with corresponding SUV values well above background activity, even in the liver. We therefore believe that the most optimal use of MR_{FDG} imaging may be in patients with less fast-growing hepatic pathologies such as low-malignant lymphomas (e.g. splenic marginal zone lymphoma) or even inflammatory diseases (sarcoidosis or infection). As we observed in our CNR analysis (Fig. 6), conditions of high background SUV coupled with low TBR(SUV) were associated with superior MR_{FDG} readability. However, we also observed quantitatively superior image readability in lesions with low background SUV and low TBR(SUV).

Other factors may also contribute to the similar lesion detectability between multiparametric and standard SUV imaging. Although our MR_{FDG} images were of visual good quality and lesion TBRs were better than in the SUV images, the D-WB PET imaging is still a nascent technique. It is conceivable that a novel noise pattern and the authors' relative unfamiliarity with reading MR_{FDG} images may have obscured lesion detection in the MR_{FDG} images. Lesions and surrounding normal tissues in different organs can reach steady state between blood and tissue at different time scales, and the tissues can

exhibit varying degree of reversible kinetics with considerable rates of dephosphorylation, as in liver tissue, which can lead to biased MR_{FDG} estimates. Additionally, we found that noise and artefacts, e.g. caused by lesion motion, can affect SUV, MR_{FDG} and DV_{FDG} differently. Thus, optimal visual reading of the combined set of SUV, MR_{FDG} and DV_{FDG} images is a challenging task. In this context, it should be noted that the image reconstruction parameters for 60–70-min SUV imaging have been thoroughly optimized, e.g. using experience from phantom experiments, whereas parameters for multiparametric imaging, such as reconstruction parameters and the timing of the WB passes, could potentially be adjusted to obtain better contrast-to-noise.

Some limitations of the study must be acknowledged. First, patients were selected primarily based on a quick evaluation of whether they were deemed fit to lie still in the PET scanner for the 70-min duration of the scan. The composition of the patient cohort in terms of referral indications is therefore not as diverse as we would have preferred and results are consequently not immediately applicable to any clinical setting. In particular, we would have liked to include patients with poorly controlled diabetes to observe, whether MR_{FDG} may add to lesion detectability under conditions of high background activity caused by hyperglycaemia. It is possible that TBR(MR_{FDG}) is better than TBR(SUV) in patients with poorly controlled diabetes and corresponding high blood glucose levels. Finally, the patient cohort represents our first experiences with positioning the patients, and movement artefacts were therefore a problem in the MR_{FDG} images. Shorter D-WB MR_{FDG} protocols will probably overcome this problem.

In this study, MR_{FDG} images were calculated from 30-min PET data as compared with 10-min SUV images. Thus, the standard static examination is clearly faster and simpler to perform with higher throughput in the daily clinic than the fully automated D-WB protocol. However, our study shows that it is possible to incorporate a D-WB protocol as part of the daily clinic, where we routinely scan several patients weekly. Still, the D-WB PET examination time could be shortened to only include the final passes needed for multiparametric reconstruction, which can be accomplished by replacing the image-derived (aorta) input function with a population-based input function scaled to the late time points in the aorta. This

Table 3 Advantages and disadvantages of D-WB FDG PET/CT

Advantages	Disadvantages
<ul style="list-style-type: none"> • Contains both the static SUV image and multiparametric images (MR_{FDG}, DV_{FDG}) in the same examination • Potential for more precise quantification of tumour metabolism and treatment response • Improved image readability due to better TBR and CNR • Fewer false-positive findings 	<ul style="list-style-type: none"> • Longer acquisition protocol • Increased sensitivity to patient movement • Altered overall PET image appearance and lesion-to-background patterns necessitating training of reading physicians • New technology that still needs further optimization (scan protocol, image reconstruction) and validation for different patient groups and radiotracers

will be a major aim of the ongoing optimization of the technique. It is our belief that we will be able to shorten the current D-WB PET scan protocol to 30 min—and with the sensitivity of contemporary PET scanners, useful D-WB protocols could probably be as short as 20 min. Further studies are needed to address whether the use of population-based input functions is robust and applicable to all patient groups. A short 20-min scan protocol is more likely to be tolerated by all patients and would be less prone to motion artefacts in the multiparametric images caused by organ and lesion movement between WB passes during extended examinations. Ideally, further development of multiparametric PET imaging should include motion compensation to allow completely aligned images of SUV, MR_{FDG} and DV_{FDG}. Taken together, the D-WB FDG PET/CT is more time-consuming than a standard static clinical scan and therefore less comfortable to the patients, and it will reduce the total patient throughput if applied to more than the first patient of the day. Thus, based on our findings, we do not think that D-WB should be used in a broad clinical context, but rather as a technique to accurately monitor treatment response or in select patient groups, where the trade-off between the longer scan time and the benefits to patients is justified. D-WB MR_{FDG} imaging may allow for robust treatment response evaluation by PET, which is today largely confined to malignant lymphomas and experimental protocols. In malignant lymphomas, FDG activity in residual tissue is rated as pathological if lesion radioactivity (the SUV_{max}) is above liver activity [26]. In essence, this is still a subjective and visual evaluation based on measurements of SUV in lesions and often ill-defined areas and volumes of the liver. In addition, lesion and liver SUV_{max} may differ substantially according to the scanning and image reconstruction preferences of individual PET institutions [27]. As a result, patients may be classified differently depending on how and where they are PET scanned. Multiparametric PET imaging contains more information about tracer kinetics and is therefore less susceptible to signal differences arising from these limitations related to static SUV imaging. An actual threshold for what constitutes pathological FDG uptake may therefore be established. These advantages of D-WB MR_{FDG} imaging as well as the disadvantages outlined above are summarized in Table 3.

To conclude, D-WB FDG PET/CT imaging is feasible in a clinical setting and produces MR_{FDG} images that are characterized by superior lesion target-to-background ratio, fewer false-positive findings and good lesion contrast-to-noise when compared with standard SUV images. However, acquiring the full data set in D-WB PET is more laborious than conventional SUV FDG PET/CT imaging and MR_{FDG} revealed no additional malignant lesions in our mixed cohort of patients referred to FDG PET/CT. Until the D-WB FDG PET/CT examination has been shortened, it should probably be reserved for

select indications such as slow-growing pathologies and possibly treatment response evaluation, where MR_{FDG} images complement the standard SUV images, enhance image reading and provide robust quantification.

Authors' contributions A.H.D. analysed images, performed statistics and wrote the final version of the manuscript; M.F.P. and H.D. performed all D-WB PET scans; A.H.D., O.L.M. and L.C.G. conceived the study; A.H.D., O.L.M. and L.C.G. wrote the first draft; A.H.D., M.F.P., H.D., O.L.M. and L.C.G. revised the manuscript and approved of the final version.

Funding The study was funded by an unrestricted grant (NNF19OC0055100) from The Novo Nordisk Foundation (to L.C.G.).

Availability of data and material All data are available from the authors upon reasonable request.

Compliance with ethical standards

Conflict of interest The authors declare that they have no conflict of interest.

Ethics approval Access to patient files was granted by the Danish Patient Safety Authority (31-1521-59) and the institutional review board at the Aarhus University Hospital.

Consent to participate Due to the retrospective nature of the study, individual patient consent was waived by the local ethics committee at Region Midtjylland and Aarhus University Hospital.

References

1. Juweid ME, Cheson BD. Positron-emission tomography and assessment of cancer therapy. *N Engl J Med*. 2006;354:496–507. <https://doi.org/10.1056/NEJMra050276>.
2. Weber WA. Positron emission tomography as an imaging biomarker. *J Clin Oncol*. 2006;24:3282–92. <https://doi.org/10.1200/jco.2006.06.6068>.
3. Weber WA, Wieder H. Monitoring chemotherapy and radiotherapy of solid tumors. *Eur J Nucl Med Mol Imaging*. 2006;33(Suppl 1): 27–37. <https://doi.org/10.1007/s00259-006-0133-3>.
4. Boellaard R, Delgado-Bolton R, Oyen WJ, Giammarile F, Tatsch K, Eschner W, et al. FDG PET/CT: EANM procedure guidelines for tumour imaging: version 2.0. *Eur J Nucl Med Mol Imaging*. 2015;42:328–54. <https://doi.org/10.1007/s00259-014-2961-x>.
5. Wahl RL, Jacene H, Kasamon Y, Lodge MA. From RECIST to PERCIST: evolving considerations for PET response criteria in solid tumors. *J Nucl Med*. 2009;50(Suppl 1):122s–50s. <https://doi.org/10.2967/jnumed.108.057307>.
6. Keyes JW Jr. SUV: standard uptake or silly useless value? *J Nucl Med*. 1995;36:1836–9.
7. Boellaard R, Krak NC, Hoekstra OS, Lammertsma AA. Effects of noise, image resolution, and ROI definition on the accuracy of standard uptake values: a simulation study. *J Nucl Med*. 2004;45: 1519–27.
8. Thie JA. Understanding the standardized uptake value, its methods, and implications for usage. *J Nucl Med*. 2004;45:1431–4.

9. Sarikaya I, Sarikaya A, Sharma P. Assessing the effect of various blood glucose levels on (18)F-FDG activity in the brain, liver, and blood Pool. *J Nucl Med Technol*. 2019;47:313–8. <https://doi.org/10.2967/jnmt.119.226969>.
10. Sprinz C, Altmayer S, Zanon M, Watte G, Irion K, Marchiori E, et al. Effects of blood glucose level on 18F-FDG uptake for PET/CT in normal organs: a systematic review. *PLoS One*. 2018;13:e0193140. <https://doi.org/10.1371/journal.pone.0193140>.
11. Lindholm P, Minn H, Leskinen-Kallio S, Bergman J, Ruotsalainen U, Joensuu H. Influence of the blood glucose concentration on FDG uptake in cancer—a PET study. *J Nucl Med*. 1993;34:1–6.
12. Ter-Pogossian MM. Special characteristics and potential for dynamic function studies with PET. *Semin Nucl Med*. 1981;11:13–23. [https://doi.org/10.1016/s0001-2998\(81\)80049-9](https://doi.org/10.1016/s0001-2998(81)80049-9).
13. Rahmim A, Lodge MA, Karakatsanis NA, Panin VY, Zhou Y, McMillan A, et al. Dynamic whole-body PET imaging: principles, potentials and applications. *Eur J Nucl Med Mol Imaging*. 2019;46:501–18. <https://doi.org/10.1007/s00259-018-4153-6>.
14. Karakatsanis NA, Lodge MA, Tahari AK, Zhou Y, Wahl RL, Rahmim A. Dynamic whole-body PET parametric imaging: I. Concept, acquisition protocol optimization and clinical application. *Phys Med Biol*. 2013;58:7391–418. <https://doi.org/10.1088/0031-9155/58/20/7391>.
15. Karakatsanis NA, Lodge MA, Yun Z, Mhlanga J, Chaudhry MA, Tahari AK, et al. Dynamic Multi-Bed FDG PET imaging: feasibility and optimization. *IEEE*. 2011:3863–70.
16. Patlak CS, Blasberg RG, Fenstermacher JD. Graphical evaluation of blood-to-brain transfer constants from multiple-time uptake data. *J Cereb Blood Flow Metab*. 1983;3:1–7. <https://doi.org/10.1038/jcbfm.1983.1>.
17. Patlak CS, Blasberg RG. Graphical evaluation of blood-to-brain transfer constants from multiple-time uptake data. Generalizations. *J Cereb Blood Flow Metab*. 1985;5:584–90. <https://doi.org/10.1038/jcbfm.1985.87>.
18. de Geus-Oei LF, Visser EP, Krabbe PF, van Hoom BA, Koenders EB, Willemsen AT, et al. Comparison of image-derived and arterial input functions for estimating the rate of glucose metabolism in therapy-monitoring 18F-FDG PET studies. *J Nucl Med*. 2006;47:945–9.
19. Wang G, Qi J. Direct estimation of kinetic parametric images for dynamic PET. *Theranostics*. 2013;3:802–15. <https://doi.org/10.7150/thno.5130>.
20. Fahmi G, Karakatsanis NA, Di Domenicantonio G, Garibotto V, Zaidi H. Does whole-body Patlak (18)F-FDG PET imaging improve lesion detectability in clinical oncology? *Eur Radiol*. 2019;29:4812–21. <https://doi.org/10.1007/s00330-018-5966-1>.
21. Danielsen H, Pedersen MF, Gormsen LC, Munk OL. Parametric whole body FDG PET scan: Just Do It! . in Annual Congress of the European Association of Nuclear Medicine October 2019 Barcelona, Spain. *Eur J Nucl Med Mol Imaging*. 2019:885.
22. Tao Y, Peng Z, Krishnan A, Zhou XS. Robust learning-based parsing and annotation of medical radiographs. *IEEE Trans Med Imaging*. 2011;30:338–50. <https://doi.org/10.1109/tmi.2010.2077740>.
23. Wang G, Qi J. Acceleration of the direct reconstruction of linear parametric images using nested algorithms. *Phys Med Biol*. 2010;55:1505–17. <https://doi.org/10.1088/0031-9155/55/5/016>.
24. Karakatsanis NA, Lodge MA, Zhou Y, Wahl RL, Rahmim A. Dynamic whole-body PET parametric imaging: II. Task-oriented statistical estimation. *Phys Med Biol*. 2013;58:7419–45. <https://doi.org/10.1088/0031-9155/58/20/7419>.
25. Kokudo N, Tada K, Seki M, Ohta H, Azekura K, Ueno M, et al. Proliferative activity of intrahepatic colorectal metastases after pre-operative hemihepatic portal vein embolization. *Hepatology*. 2001;34:267–72. <https://doi.org/10.1053/jhep.2001.26513>.
26. Cheson BD, Fisher RI, Barrington SF, Cavalli F, Schwartz LH, Zucca E, et al. Recommendations for initial evaluation, staging, and response assessment of Hodgkin and non-Hodgkin lymphoma: the Lugano classification. *J Clin Oncol*. 2014;32:3059–68. <https://doi.org/10.1200/jco.2013.54.8800>.
27. Ly J, Minarik D, Edenbrandt L, Wollmer P, Tragardh E. The use of a proposed updated EARL harmonization of (18)F-FDG PET-CT in patients with lymphoma yields significant differences in Deauville score compared with current EARL recommendations. *EJNMMI Res*. 2019;9:65. <https://doi.org/10.1186/s13550-019-0536-3>.

Publisher's note Springer Nature remains neutral with regard to jurisdictional claims in published maps and institutional affiliations.